Performance Analysis of a Diffusion Control Method for ANC Systems and the Network Design

Y. J. Chu[a], C. M. Mak[b], Y. Zhao[a], S. C. Chan[c], and M. Wu[d]

[a] *State Key Laboratory of Subtropical Building Science, South China University of Technology*
[b] *Department of Building Services Engineering, The Hong Kong Polytechnic University*
[c] *Department of Electrical Electronics Engineering, The University of Hong Kong*
[d] *Key Laboratory of Noise and Vibration Research, Institute of Acoustics, China*

Abstract—Active noise control (ANC) systems have been widely used to reduce noise from indoor or outdoor sources, e.g. traffic, office/factory machines and ventilating systems. Since noise control usually needs to be executed within an extended area, the ANC network that involves a large amount of error microphones and loudspeakers is frequently employed. Distribution of the controller network saves computational burden and yields spatial diversity, which enhances the robustness of the system. This paper studies the diffusion (Diff) control for multi-channel ANC systems using filtered-x (Fx) least mean squares (LMS) algorithms. Since communication between nodes within the network makes it difficult to analyze the performance of the entire system, a comprehensive performance analysis of networked FxLMS algorithm is not available currently in literature to our best knowledge. In this paper, the convergence behavior of the Diff-FxLMS algorithm is investigated. The mean and mean squares difference equations are derived, from which the stability of the networked ANC system is analyzed and the steady-state excess mean square errors (EMSEs) for ANC controllers are obtained. Computer simulations are conducted to compare different control methods and verify the theoretical analysis. A specific 10-node network is studied in terms of the network strategy and the noise reduction performance. Moreover, using the proposed theoretical analysis, a systematic and simple design procedure for Diff-FxLMS based ANC systems is proposed. The usefulness of the theoretical analysis and design procedure is demonstrated by means of a design example.

Keywords—Active noise control (ANC), diffusion control, performance analysis, and network design.

1. Introduction

Active control of noise usually involves a large number of loudspeakers and error microphones in order to achieve the global control over a region of space [1]. Such a system, called the multi-channel active noise control (ANC) system, is frequently used to improve the quality of sound environment by preventing sound propagation over an open area, e.g. openings in walls [2][3] or over open-plan office barriers [4] that enable sound to propagate and deteriorate indoor environmental quality and human comfort [5].

However, conventional ANC systems use a group of single-channel controllers where each controller is working independently to attenuate the local noise level [6]. One problem with such systems is that it is difficult to achieve a global optimization of noise reduction in a large area [7]. In order to have a global control of noise by means of the multi-channel ANC systems, a so called multiple error (ME) ANC algorithm [1] is proposed. One of the most widely used MEANC algorithms is based on the filtered-x least mean squares (FxLMS) algorithm [8] and its variants [9]-[11]. Several control methods for multiple error FxLMS (MEFxLMS) algorithms are developed, e.g., the centralized, decentralized, and distributed strategies. Centralized processing [1] has been proved to perform very well. However, it is quite computationally consuming, since each controller needs to process signal from all the secondary sources and the centralized ANC system needs to process K^2 transfer functions (K is the number of loudspeakers/error microphones). A technique called the decentralized control has been developed to reduce complexity and facilitate hardware design of multi-channel control systems [12]. Instead of dealing with the global error received by all the K error microphones, each controller minimizes the error power at one cancellation point only. Decentralized systems are able to decrease computational burden from order K^2 to K. However, they cannot outperform centralized systems in most cases and may bring in the major drawback of the increased risk of global instability [13]. A lot of effort has been taken to derive a sufficient stability condition [14][15] for such systems or to employ the feedforward structure [16].

As an alternative, a new MEFxLMS algorithm using an incremental collaborative strategy [17] as shown in Fig. 1(a) (cited from [18]) is proposed in [19]. This algorithm allows communication between controllers

such that it is more robust than the decentralized ANC algorithm. The incremental control, however, suffers from several drawbacks for real-time adaptation over networks, such as the sensitivity to the failure of a single node, the limited data communication between nodes, and the fixed simple cyclic path for incremental steps [20]. To overcome these problems, a diffusion strategy [21], as shown in Fig. 1(b), has been employed and some new diffusion MEFx-like ANC algorithms have been proposed recently in [18].

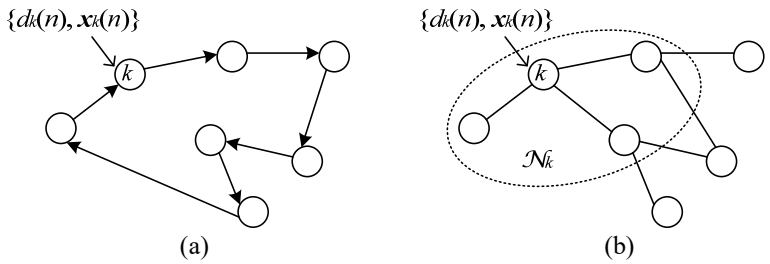

Fig. 1. Distributed network of node k: (a) an incremental structure where nodes update along a cyclic loop, and (b) a diffusion structure where nodes communicate within a neighborhood $\mathcal{N}_k$. Node k collects the data set $\{d_k(n), \boldsymbol{x}_k(n)\}$ at time index n. (cited from [18]).

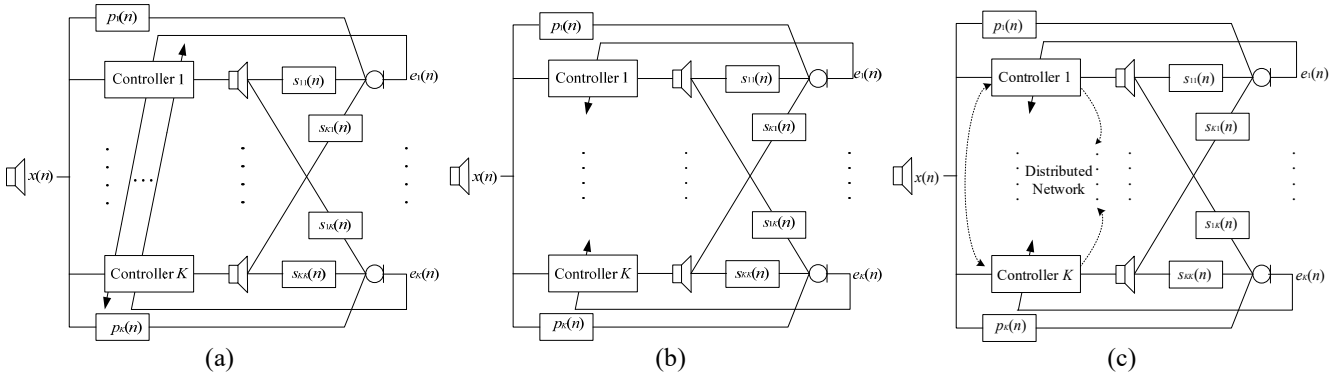

Fig. 2. Block diagram of ANC systems with different control strategies: (a) centralized; (b) decentralized; and (c) distributed (cited from [18]).

The diffusion strategy is compared with conventional methods in Fig. 2. It can be seen that each controller deals with signals picked up by all error microphones in the centralized strategy while the decentralized controller only processes signals from one error microphone. Therefore, the decentralized structure could reduce the complexity by one order. The distributed strategy also processes signals from one microphone such that it has a complexity comparable to the distributed strategy. It further combines the controller parameters according to a certain combination rule, which increases the system robustness without involving any extra multiplication. The reason for the improved performance is to be disclosed in Section 3.

Recently, a lot of attention has been paid to developing more efficient distributed adaptive algorithms in ANC systems. The distributed transform domain (TD) and affine projection algorithms (APAs) have been employed to increase convergence of controllers in multi-channel ANC systems [22] [23]. In [23], the mean and mean squares deviation performance of a distributed APA for ANC is derived. However, there is few work on analyzing performance of distributed ANC algorithms that provides valuable guideline for ANC system design [24]. To our best knowledge, a detailed theoretical analysis of distributed ANC networks on important issues such as optimal solutions, convergence conditions [25], effect of combination topology on ANC networks (the so called multitask problem) [26] is unavailable. Driven by practical advantages of ANC networks, this paper is devoted to bridge this gap in the literature and address the aforementioned issues. Using the proposed theoretical analysis, a systematic and simple design procedure for ANC networks is proposed. The usefulness of the theoretical results and design procedure is demonstrated by means of a system design example. Computer simulations are also conducted to compare different control methods and verify the theoretically analysis. Moreover, a specific 10-node network is studied in terms of the diffusion strategy and noise reduction performance.

To provide valuable insight and practical guidelines for future multi-channel ANC system design, the mean and mean squares convergence performance of the Diff-FxLMS algorithm are analyzed. Difference equations describing the mean and mean squares convergence behaviors of the controller are derived, from which the convergence conditions and analytical expressions of the steady-state excess mean square error (EMSE) are derived. It shows that the diffusion strategy introduces a bias to the Wiener solution in exchange for an improved robustness of the system. It should be noted that different from the basic idea of Diff control and brief simulation results in our previous work [18], the performance analysis abovementioned is provided and verified in this paper. In addition, a specific case study of active noise control is conducted and a design method for ANC network is presented.

The rest of the paper is organized as follows: in Section 2, the conventional diffusion FxLMS algorithm for ANC networks is reviewed. The mean and mean squares convergence analysis of this algorithm is derived

and verified in Section 3. In addition, a system design method is presented. More simulations are carried out in Section 4 to examine the efficiency of different control strategies. A case study for a 10-node network is presented and the proposed system design method is examined. Finally, conclusions are drawn in Section 5.

2. Review of Diff-FxLMS Algorithm

Fig. 3 shows the diagram of an ANC system using the Fx algorithm. For a certain channel, say the *k*th channel, the undesirable noise at the error microphone $\{d_{0k}(n)\}$ is to be cancelled by an acoustic signal $\{y_k(n)\}$. $\{d_{0k}(n)\}$ is generated from the noise source signal $\{x(n)\}$ through the primary path $\{p_k(n)\}$; while $\{y_k(n)\}$ is generated from a loudspeaker through an adaptive filter-based controller. An error microphone is used to pick up the *k*th residual signal $\{e_k(n)\}$ to be minimized. Here, *n* denotes the time instant. The acoustic path from the *i*th loudspeaker to the *j*th microphone is called the *ij*th secondary path $\{s_{ij}(n)\}$, which is modeled as finite impulse responses (FIRs). In Fig. 3, only $\{s_{kk}(n)\}$ has been shown explicitly. Secondary paths from other loudspeakers result in an interference $\{\gamma_k(n)\}$ at the *k*th microphone.

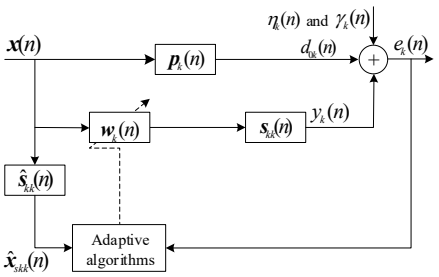

Fig. 3. Block diagram of the ANC system using the Fx-based adaptive algorithm.

According to Fig. 3, the *k*th microphone that receives the unwanted noise $d_k(n)$ and the output of the *k*th loudspeaker $y_k(n)$ reads

$$e_k(n) = d_k(n) + y_k(n). \tag{1}$$

The noise signal $d_k(n)$ contains the contribution of the source $x(n)$ through the *k*th primary path $\{p_k(n)\}$, namely $d_{0k}(n)$, the background noise $\eta_k(n)$, and the interference $\gamma_k(n)$ from the other secondary sources except the *k*th one. Thus, $\{d_k(n)\}$ can be expressed as

$$d_k(n) = d_{0k}(n) + \eta_k(n) + \gamma_k(n). \tag{2}$$

Define the discrete time convolution "*". We further have the controller output $y_k(n) = x(n) * w_k(n) * s_{kk}(n)$, the noise signal $d_{0k}(n) = p_k(n) * x(n)$, and the interference $\gamma_k(n) = \sum_{l \neq k, l=1}^{K} x(n) * w_l(n) * s_{lk}(n)$. To minimize the power of $\{e_k(n)\}$, the controller $\{w_k(n)\}$ aims to approximate $\{-p_k(n)\}$ after cascading with $\{s_{kk}(n)\}$. Using the property that the discrete-time convolution is commutative, the filtered signal $x_{slk}(n) = x(n) * s_{lk}(n)$ can be used as the input of the adaptive filter. Since $\{s_{lk}(n)\}$ is unknown, it is replaced by the estimate $\{\hat{s}_{lk}(n)\}$ and the filter input is actually $\hat{x}_{slk}(n) = x(n) * \hat{s}_{lk}(n)$ for $l, k = 1, \ldots, K$. It can be seen that the filtered input is different when nodes are distributed at different locations. Moreover, the true solution to each node deviates from each other, which results in the multitask problem in ANC networks.

Conventional FxLMS that uses the Combine Then Adapt (CTA) diffusion strategy [20], namely the CTA-FxLMS algorithm [18], can be summarized as

$$\boldsymbol{w}_k(n) = \sum_{l \in \mathcal{N}_k} a_{lk} \boldsymbol{\psi}_l(n) \tag{3}$$

$$\boldsymbol{\psi}_k(n+1) = \boldsymbol{w}_k(n) - \mu_k \hat{\boldsymbol{x}}_k(n) e_k(n) \tag{4}$$

where $\mu_k > 0$ is the local step-size, $\hat{\boldsymbol{x}}_k(n) = [\hat{x}_{skk}(n), \ldots, \hat{x}_{skk}(n-L+1)]^T$ is the filtered input vector, and L is the length of the adaptive filter for the ANC controller $\{w_k(n)\}$. $\boldsymbol{\psi}_l(n)$ is the local estimates, which are fused at node k over the neighborhood $l \in \mathcal{N}_k$. The combination weights a_{lk} satisfy $\sum_{l \in \mathcal{N}_k} a_{lk} = 1$. Compared to the decentralized control, the combination provides information from other nodes. It is a tradeoff between the centralized and decentralized control, which could increase the system robustness without involving any extra multiplication. The reason for the improved performance is to be disclosed in Section 3 (stability conditions) and simulations are conducted to verify the statement in Section 4 (Fig. 8).

3. Performance Analysis of Diff-FxLMS Algorithm

We are interested in studying the mean and mean squares convergence behaviors of the cooperative system. First, from the mean convergence analysis, we show how cooperation changes the optimal solution to

each controller [see (7) and (8)], which deviates from the true value (Wiener Solution) and causes the multitask problem. As a tradeoff, cooperation has a stabilizing effect on the network. Then, we proceed to perform the mean squares analysis that characterizes the residual noise at each node and the evolution of its learning curves [refer to (16)], as well as derive the estimation deviation in terms of EMSE. The performance analysis gains insight into the mechanism of ANC networks and provides useful guidance to algorithm development and system design. In addition, based on the analysis, user parameters can be selected automatically without the computational consuming try-and-error method.

Even for single channel ANC controllers, several simplifying assumptions have to be adopted to make the performance analysis of ANC algorithms mathematically available [24]. The challenges are compounded in ANC networks because the dynamic and interconnected collection of nodes influences each other's behavior. To proceed with the analysis, we therefore introduce similar assumptions as in traditional adaptive literature. The assumptions made to facilitate the performance analysis are as follows:

(A1) the filtered input signal $\{\hat{x}_{sij}(n)\}$ is the zero-mean Gaussian random signals;

(A2) $\boldsymbol{x}_k(n)$, $\boldsymbol{w}_k(n)$ and $\eta_k(n)$ are statistically independent; so is the estimated filtered input $\hat{\boldsymbol{x}}_k(n)$;

(A3) the interference $\{\gamma_k(n)\}$ is weakly correlated with the filtered input $\{x_{skk}(n)\}$.

(A2) is the independence assumption, commonly used in analyzing adaptive algorithms [27][28]. It is quite accurate for large filter length and small to medium step-sizes.

To have a concise expression in the following analysis, we resort to state-space representations and define the global quantities

$$\boldsymbol{\psi}_C(n) = \mathrm{col}\{\boldsymbol{\psi}_1(n),...,\boldsymbol{\psi}_K(n)\}\ (LK \times 1),\ \boldsymbol{w}_C(n) = \mathrm{col}\{\boldsymbol{w}_1(n),...,\boldsymbol{w}_K(n)\}\ (LK \times 1)$$

$$\boldsymbol{e}(n) = \mathrm{col}\{e_1(n),...,e_K(n)\}\ (K \times 1),\ \hat{\boldsymbol{\mathcal{X}}}(n) = \mathrm{diag}\{\hat{\boldsymbol{x}}_1(n),...,\hat{\boldsymbol{x}}_K(n)\}\ (LK \times K)$$

in terms of the stochastic quantities that appear in the update equations (3) and (4). Here, col{} and diag{} format the elements as a column vector or block diagonal matrix. Using the above representations, the measurement in (1) is assumed to obey a linear model as

$$\boldsymbol{e}(n) = \boldsymbol{d}(n) + \boldsymbol{X}^T(n)\boldsymbol{w}_C(n) \tag{5}$$

where $\boldsymbol{d}(n) = \text{col}\{d_1(n),...,d_K(n)\}$ is a vector of size K, and the reference signal received by the error microphone can be expressed as $\boldsymbol{X}(n) = \text{diag}\{\boldsymbol{x}_1(n),...,\boldsymbol{x}_K(n)\}$ ($LK \times K$). Let

$$\boldsymbol{D}_\mu(n) = \text{diag}\{\mu_1\boldsymbol{I}_L,...,\mu_K\boldsymbol{I}_L\}$$

be the block diagonal matrix of dimension $LK \times LK$ that collects the local step-sizes. With these expressions, Eqs. (3) and (4) admit the following global representation

$$\boldsymbol{\psi}_C(n+1) = \boldsymbol{G}\boldsymbol{\psi}_C(n) - \boldsymbol{D}_\mu\hat{\boldsymbol{X}}(n)\boldsymbol{e}(n) \tag{6}$$

where $\boldsymbol{G} = \boldsymbol{A}^T \otimes \boldsymbol{I}_L$ is the $LK \times LK$ network topology matrix, $\otimes$ is the Kronecker product, and the combining matrix $\boldsymbol{A}$ is formed by $\{a_{lk}\}$ for $l, k = 1,\ldots,K$. Without loss of generality, we assume a symmetric combining matrix such that we have $\boldsymbol{G} = \boldsymbol{G}^T$ in the rest of the paper.

3.1 Mean convergence analysis

In the mean convergence analysis, the optimal solution to the networked ANC system is obtained, and the mean convergence speed as well as the mean convergence condition is examined.

We assume that the algorithm is convergent, i.e. $\boldsymbol{\psi}_C(n)$ converges to $\boldsymbol{\psi}_\infty$ and $\boldsymbol{w}_C(n)$ converges to $\boldsymbol{w}_\infty$. At the steady state, taking expectations of both sides of (6) leads to the solution $\boldsymbol{\psi}_\infty$

$$\boldsymbol{\psi}_\infty = -[\boldsymbol{R}_{\hat{X}X}\boldsymbol{G} + \boldsymbol{D}_\mu^{-1}(\boldsymbol{I}_{LK} - \boldsymbol{G})]^{-1}\boldsymbol{r}_{\hat{X}d} \tag{7}$$

where $\boldsymbol{R}_{\hat{X}X} = E[\hat{\boldsymbol{X}}(n)\boldsymbol{X}^T(n)]$ is the covariance matrix and $\boldsymbol{r}_{\hat{X}d} = E[\hat{\boldsymbol{X}}(n)\boldsymbol{d}(n)]$ is the cross-correlation vector. Then the global solution finds from (3)

$$\boldsymbol{w}_\infty = -\boldsymbol{G}[\boldsymbol{R}_{\hat{X}X}\boldsymbol{G} + \boldsymbol{D}_\mu^{-1}(\boldsymbol{I}_{LK} - \boldsymbol{G})]^{-1}\boldsymbol{r}_{\hat{X}d}. \tag{8}$$

It can be seen that the first term in the brackets of both (7) and (8) is related to the Wiener solution. An estimation bias (the second term in the brackets) is introduced by the network topology. The controller at each node $\boldsymbol{\psi}_k(n)$ converges to different steady-state values and the relationship $\boldsymbol{\psi}_\infty = \boldsymbol{G}\boldsymbol{\psi}_\infty$ no longer holds. This is called the multitask problem [26] in ANC systems.

To find the Wiener solution to the conventional multi-channel FxLMS-based ANC controller $\boldsymbol{w}_0$, we let $\boldsymbol{G} = \boldsymbol{I}_{LK}$. This means there is no combination between neighbouring nodes. Consequently, Eq. (8) reduces to

$$\boldsymbol{w}_0 = \boldsymbol{G}\boldsymbol{\psi}_0 = -\boldsymbol{R}_{\hat{X}X}^{-1}\boldsymbol{r}_{\hat{X}d} \tag{9}$$

where $\boldsymbol{w}_0 = \text{col}\{\boldsymbol{w}_{01},...,\boldsymbol{w}_{0K}\}$ is a vector of size ($LK \times 1$).

Define the bias of the controller $\Delta\boldsymbol{\psi} = \boldsymbol{\psi}_0 - \boldsymbol{\psi}_\infty$. It finds from (7)-(9) that

$$\boldsymbol{R}_{\hat{X}X}\boldsymbol{G}\Delta\boldsymbol{\psi} = \boldsymbol{D}_\mu^{-1}(\boldsymbol{I}_{LK} - \boldsymbol{G})\boldsymbol{\psi}_\infty . \tag{10}$$

It shows that this bias is related to the step-sizes and network topology.

The effect of the combining strategy on the optimal solution [see (8)] has been investigated and verified in Fig. 4. In this experiment, short primary and secondary paths are considered for theoretical analysis use. The length of primary paths and the controllers is set to 11. The length of secondary paths is 3. The same Metropolis matrix is used as the combination coefficients in the ANC network. The primary paths $\boldsymbol{p}_i$ are randomly distributed on a circle of radius r centered at $\boldsymbol{p}_0$, i.e. $\boldsymbol{p}_i = \boldsymbol{p}_0 + r\boldsymbol{g}_i$, for i = 1, 2,…, and $\boldsymbol{g}_i$ is a Gaussian sequence of unit norm. The noise is supposed to be white Gaussian sequences and the signal-to-noise ratio (SNR), defined as $10\log\{\text{var}[d_{0k}^2(n)]/\text{var}[\eta_k^2(n)]\}$, at the receiver error microphone is set to 20 dB.

In Fig. 4(a), a 10-node ANC network is considered and we verify the optimal solution by using the norm of mean weight-error vector $\|\boldsymbol{v}^\Delta(n)\|_2^2$ for $\Delta = 0$ or ∞. The weight-error vectors that measure the distance between the estimate and the Wiener (9) or optimal (8) solutions are defined as 1) $\boldsymbol{v}^0(n) = \overline{\boldsymbol{w}}_C(n) - \boldsymbol{w}_0(n)$ and 2) $\boldsymbol{v}^\infty(n) = \overline{\boldsymbol{w}}_C(n) - \boldsymbol{w}_\infty$. The radius r is set to 0 (black lines), 0.05 (blue lines), and 0.1 (red lines) to form different multitask problems. The step-size for CTA-FxLMS is set to 0.01 and 0.002 to test the effect of step-sizes on the optimal solution. It can be seen that the optimal solution curves (all the 6 solid lines) converge to a similar value at the steady state, which is comparable to the Wiener solution curve at r = 0 (the 2 dash-dot lines for r = 0). Moreover, the Wiener solution curves (dash-dot lines) overlap with the optimal

solution curves (solid line) when the radius is 0. As the radius increases, the Wiener solution curves converge to a higher steady-state value in each step-size group. It shows that, for multitask problems, the controllers converge to the derived optimal solution in (8) rather than the Wiener solution in (9). For the smaller step-size μ = 0.002, similar phenomena can be observed. Comparing the 2 red dash-dot lines (or the 2 blue dash-dot lines), where the radius is the same while the step-size is different, it can be seen that the estimation bias increases slightly with the step-size [as indicated in (10)]. Next, we examine the effect of number of nodes on the estimation bias $|\Delta\boldsymbol{\psi}|^2$ under a specific condition, where the step-size is set to 0.01 and the radius is 0.1. The number of nodes is set to 1, 5, 10, 15, and 20. The other settings are the same as in Fig. 4(a) if not specified. As shown in Fig. 4(b), the estimation bias increases with the number of nodes.

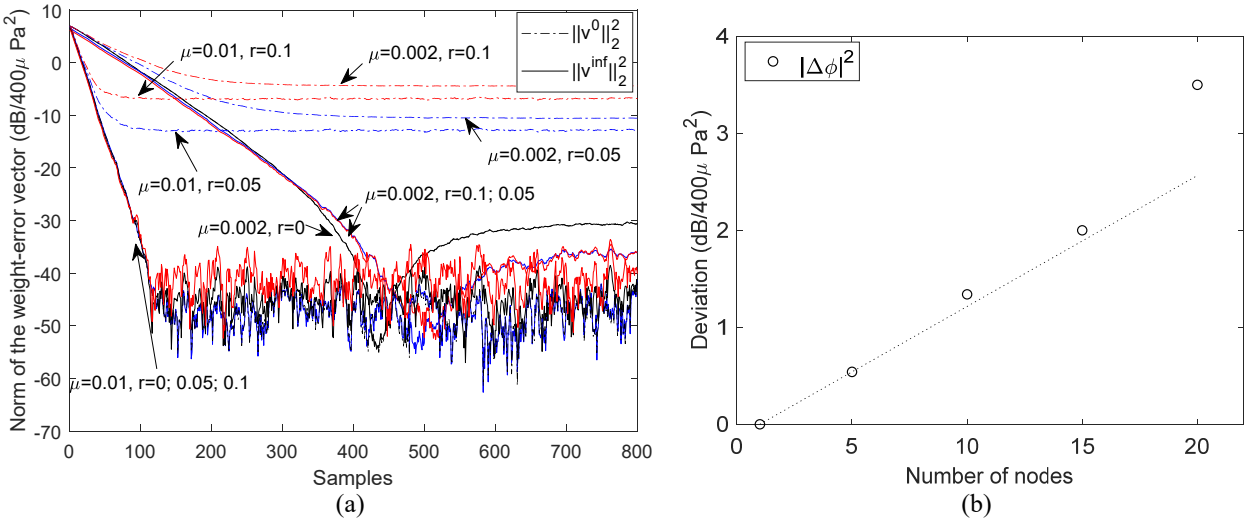

Fig. 4. (a) Learning curves of the norm of mean weight-error vectors under different settings. K = 10. (b) Estimation bias of ANC networks using different number of nodes.

In the following, we study the mean convergence condition of the network and show how cooperation stabilizes the algorithm. Introduce the global weight error vectors $\boldsymbol{v}(n) = \boldsymbol{\psi}_\infty - \boldsymbol{\psi}_C(n)$ and $\boldsymbol{v}_G(n) = \boldsymbol{G}[\boldsymbol{\psi}_\infty - \boldsymbol{\psi}_C(n)]$. Subtracting $\boldsymbol{\psi}_C(n)$ from both sides of (6), we get

$$\boldsymbol{v}(n+1) = \boldsymbol{v}_G(n) + \boldsymbol{D}_\mu \hat{\boldsymbol{X}}(n)\boldsymbol{e}(n) + (\boldsymbol{I}_{LK} - \boldsymbol{G})\boldsymbol{\psi}_\infty \tag{11}$$

Taking expectation of both sides of (11) and using the optimal solution (7), we have the following mean difference equation

$$\bar{\boldsymbol{v}}(n+1) = (\boldsymbol{I}_{LK} - \boldsymbol{D}_{\mu}\boldsymbol{R}_{\hat{X}X})\boldsymbol{G}\bar{\boldsymbol{v}}(n) \tag{12}$$

where "$\bar{u}$" denotes $E[u]$. Therefore, to maintain stability in the mean sense we must have

$$|\lambda\{(\boldsymbol{I}_{LK} - \boldsymbol{D}_{\mu}\boldsymbol{R}_{\hat{X}X})\boldsymbol{G}\}| < 1 \tag{13}$$

where $\lambda\{\cdot\}$ denotes the eigenvalues of a given matrix. The spectrum of $(\boldsymbol{I}_{LK} - \boldsymbol{D}_{\mu}\boldsymbol{R}_{\hat{X}X})\boldsymbol{G}$ must be strictly inside the unit circle. Since the radius of $(\boldsymbol{I}_{LK} - \boldsymbol{D}_{\mu}\boldsymbol{R}_{\hat{X}X})\boldsymbol{G}$ is generally smaller than that of $(\boldsymbol{I}_{LK} - \boldsymbol{D}_{\mu}\boldsymbol{R}_{\hat{X}X})$ [21][29], the network topology enforces robustness through the network topology $\boldsymbol{G}$.

3.2 Mean squares convergence analysis

In this subsection, we proceed to perform a detailed transient analysis of the ANC network [refer to (20)], characterize mean squares stability condition [see (24)], as well as derive expressions for EMSE [see (33) and (34)]. To measure the mean squares difference equation of CTA-FxLMS, we first define the weight error covariance matrices $\boldsymbol{\Xi}(n) = E[\boldsymbol{v}(n)\boldsymbol{v}^T(n)]$ and $\boldsymbol{\Xi}_G(n) = E[\boldsymbol{v}_G(n)\boldsymbol{v}_G^T(n)]$.

3.2.1 Transient performance

Recall (2) and separate the modeling error $\Delta_k(n)$ from the Wiener solution $\boldsymbol{w}_0$. Then the measurement data $d_k(n)$ can be rewritten as

$$d_k(n) = -\boldsymbol{x}_k^T(n)\boldsymbol{w}_{0k} + \Delta_k(n) + \eta_k(n) + \gamma_k(n) \tag{14}$$

where $\Delta_k(n) = d_{0k}(n) + \boldsymbol{x}_k^T(n)\boldsymbol{w}_{0k}$. The modeling error is typical for Fx-like algorithms as explained in [24][30]. To have a concise expression in the following analysis, we introduce the global quantities of size ($K \times 1$) for the measurement and noises

$$\boldsymbol{d}_0(n) = [d_{01}(n),...,d_{0K}(n)],\ \boldsymbol{\eta}_C(n) = [\eta_1(n),...,\eta_K(n)],\ \boldsymbol{\gamma}_C(n) = [\gamma_1(n),...,\gamma_K(n)].$$

Accordingly, (5) can be rewritten as

$$\boldsymbol{e}(n) = -\boldsymbol{\mathcal{X}}^T(n)\boldsymbol{G}[\boldsymbol{\psi}_0 - \boldsymbol{\psi}_C(n)] + \boldsymbol{\eta}_{\Sigma}(n) \tag{15}$$

where $\boldsymbol{\eta}_{\Sigma}(n) = \boldsymbol{\eta}_C(n) + \boldsymbol{\gamma}_C(n) + \boldsymbol{\Delta}_C(n)$ and $\boldsymbol{\Delta}_C(n) = \boldsymbol{d}_0(n) + \boldsymbol{\mathcal{X}}^T(n)\boldsymbol{w}_0$ is a column vector of $\{\Delta_k(n)\}$.

Substituting (15) for the collected noise vector in (11), we find

$$\begin{aligned}\boldsymbol{\Xi}(n+1) &= \boldsymbol{\Xi}_G(n) - \boldsymbol{D}_\mu \boldsymbol{R}_{\hat{X}X}\boldsymbol{\Xi}_G(n) - \boldsymbol{\Xi}_G(n)\boldsymbol{R}_{X\hat{X}}\boldsymbol{D}_\mu \\ &+ \boldsymbol{D}_\mu \boldsymbol{R}_{\hat{X}X}\boldsymbol{v}_G(n)\boldsymbol{\psi}_\infty^T(\boldsymbol{G}-\boldsymbol{I}_{LK})^T + (\boldsymbol{G}-\boldsymbol{I}_{LK})\boldsymbol{\psi}_\infty \boldsymbol{v}_G^T(n)\boldsymbol{R}_{X\hat{X}}\boldsymbol{D}_\mu + \boldsymbol{D}_\mu E[\boldsymbol{Q}(n) - \widetilde{\boldsymbol{R}}_\psi]\boldsymbol{D}_\mu\end{aligned} \tag{16}$$

where $\widetilde{\boldsymbol{R}}_\psi = \boldsymbol{D}_\mu^{-1}(\boldsymbol{I}_{LK}-\boldsymbol{G})\boldsymbol{\psi}_\infty\boldsymbol{\psi}_\infty^T(\boldsymbol{I}_{LK}-\boldsymbol{G})^T\boldsymbol{D}_\mu^{-1}$, and

$$\boldsymbol{Q}(n) = E[\hat{\boldsymbol{\mathcal{X}}}(n)\boldsymbol{e}(n)\boldsymbol{e}^T(n)\hat{\boldsymbol{\mathcal{X}}}^T(n)] \tag{17}$$

The last term in (16), i.e. $\widetilde{\boldsymbol{R}}_\psi$ indicates the effect of diffusion topology on the driving term.

According to the notations in Appendix A, where (17) is evaluated, we can extract the terms related to $\boldsymbol{\Xi}_G(n)$ in the correlation term (17) and have

$$\boldsymbol{Q}_\Xi(n) = 2\boldsymbol{R}_{\hat{X}X}\boldsymbol{\Xi}_G(n)\boldsymbol{R}_{X\hat{X}} + \boldsymbol{R}_{\hat{X}\hat{X}}Tr(\boldsymbol{\Xi}_G(n)\boldsymbol{R}_{XX}) \tag{18}$$

where $\boldsymbol{R}_{\hat{X}\hat{X}} = E[\hat{\boldsymbol{\mathcal{X}}}(n)\hat{\boldsymbol{\mathcal{X}}}^T(n)]$ and $\boldsymbol{R}_{XX} = E[\boldsymbol{\mathcal{X}}(n)\boldsymbol{\mathcal{X}}^T(n)]$. Moreover, the diagonal matrix of the noise variances of $\boldsymbol{\eta}_\Sigma(n)$ has been defined as

$$\boldsymbol{D}_\Sigma = \mathrm{diag}\{\sigma_{\Sigma,1}^2\boldsymbol{I}_L,...,\sigma_{\Sigma,K}^2\boldsymbol{I}_L\} \tag{19}$$

This term contributes to the effect of noises on the driving term.

Consequently, Eq. (16) can be written as [see (A.4)]

$$\begin{aligned}\boldsymbol{\Xi}(n+1) &= \boldsymbol{\Xi}_G(n) - \boldsymbol{D}_\mu \boldsymbol{R}_{\hat{X}X}\boldsymbol{\Xi}_G(n) - \boldsymbol{\Xi}_G(n)\boldsymbol{R}_{X\hat{X}}\boldsymbol{D}_\mu + \boldsymbol{D}_\mu(\boldsymbol{Q}_\Xi(n) + \boldsymbol{D}_\Sigma\boldsymbol{R}_{XX})\boldsymbol{D}_\mu \\ &+ \boldsymbol{D}_\mu(\widetilde{\boldsymbol{R}}_\psi + \widetilde{\sigma}_\psi^2\boldsymbol{R}_{\hat{X}\hat{X}})\boldsymbol{D}_\mu + \boldsymbol{D}_\mu[\boldsymbol{R}_{\hat{X}X}\boldsymbol{\Xi}_{\Sigma,G}(n)\boldsymbol{R}_{X\hat{X}} + Tr(\boldsymbol{\Xi}_{\Sigma,G}(n)\boldsymbol{R}_{XX})\boldsymbol{R}_{\hat{X}\hat{X}}]\boldsymbol{D}_\mu\end{aligned} \tag{20}$$

where $\widetilde{\sigma}_\psi^2 = Tr(\boldsymbol{R}_{XX}^{-1}\widetilde{\boldsymbol{R}}_\psi)$ and $\boldsymbol{\Xi}_{\Sigma,G}(n) = \bar{\boldsymbol{v}}_G(n)\Delta\boldsymbol{\psi}^T\boldsymbol{G} + \boldsymbol{G}^T\Delta\boldsymbol{\psi}\bar{\boldsymbol{v}}_G^T(n)$. Note, the mean error vector related terms $\bar{\boldsymbol{v}}_G(n)$ and $\boldsymbol{\Xi}_{\Sigma,G}(n)$ vanish at the steady state.

The weight error covariance matrix $\boldsymbol{\Xi}(n)$ measures the estimation deviation. Based on $\boldsymbol{\Xi}(n)$, the following global EMSE convergence curve is defined

$$\mathrm{EMSE}(n) = \tfrac{1}{K}Tr(\boldsymbol{R}_{xx}\boldsymbol{\Xi}(n)). \tag{21}$$

The EMSE convergence curves are compared with the simulation results in Fig. 5. The settings are identical to those in the previous experiment (Fig. 4). It can be seen that, generally, the theoretical and simulated global EMSE curves agree well with each other. When a large step-size is used at $r = 0$, the steady-state EMSE is overestimated slightly (see the black lines denoted with $\mu = 0.01$, $r = 0$). It also shows

that as the value of r increases, i.e. the optimal solution to each node becomes more different from each other, the steady-state EMSE becomes larger.

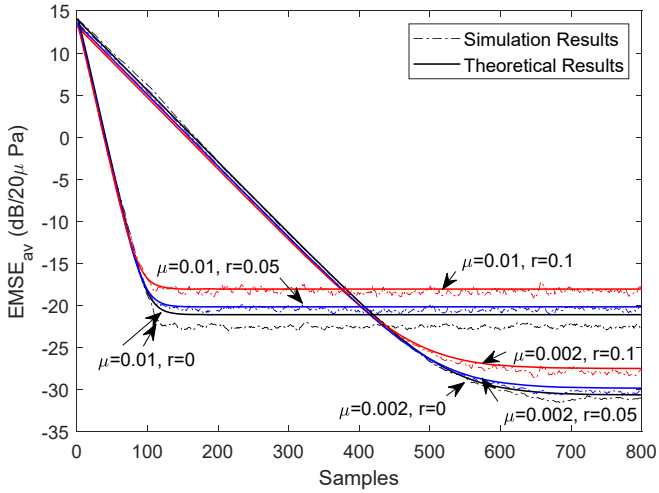

Fig. 5. Learning curves of averaged global EMSE under different settings. $K = 10$.

3.2.2 Stability condition

The stability in the mean sense requires that the step-size $\{\mu_k\}$ must satisfy (13), given a certain combination strategy. On the other hand, it shows in (20) that convergence in the mean-square sense depends on space-time data statistics such as the input covariance matrix, and the network topology. A simple procedure that is sufficient to ensure global stability is derived. First, we take the trace of both sides of (20). Then, defining the measure of energy $\varphi(n) = Tr(\boldsymbol{\Xi}(n))$ and $\varphi_G(n) = Tr(\boldsymbol{\Xi}_G(n))$, we formulate

$$\varphi(n+1) = \varphi_G(n) - 2Tr(\boldsymbol{D}_\mu \boldsymbol{R}_{\hat{X}X} \boldsymbol{\Xi}_G(n)) + \tau(n) + \tau_0(n) \tag{22}$$

where $\tau(n) = Tr(\boldsymbol{D}_\mu^2 \boldsymbol{Q}_\Xi(n))$ is a term related to $\varphi_G(n)$ and $\tau_0(n)$ is the driving term as shown below

$$\tau_0(n) = Tr(\boldsymbol{D}_\mu^2[\boldsymbol{D}_\Sigma \hat{\boldsymbol{R}}_{XX} + (\widetilde{\boldsymbol{R}}_\psi + \widetilde{\sigma}_\psi^2 \boldsymbol{R}_{\hat{X}\hat{X}}) + \boldsymbol{R}_{\hat{X}X} \boldsymbol{\Xi}_{\Sigma,G}(n) \boldsymbol{R}_{X\hat{X}} + Tr(\boldsymbol{\Xi}_{\Sigma,G}(n) \boldsymbol{R}_{XX}) \boldsymbol{R}_{\hat{X}\hat{X}}]).$$

It can be seen that $\tau_0(n)$ is related to $\bar{\boldsymbol{v}}_G$, $\boldsymbol{\psi}_\infty$, $\Delta\boldsymbol{\psi}$ and noise variances. Since they are finite, and $\bar{\boldsymbol{v}}_G$ converges to zero if the mean convergence condition (13) is satisfied, we only need to consider the terms on the right hand side of (22) that contain $\boldsymbol{\Xi}_G(n)$. After some algebraic manipulations, we have

$$\varphi(n+1) = E[\boldsymbol{v}^T \boldsymbol{G}^T \boldsymbol{F} \boldsymbol{G} \boldsymbol{v}] + \tau_0(n) \tag{23}$$

where $\boldsymbol{F} = \boldsymbol{I}_{LK} - 2\boldsymbol{D}_\mu \boldsymbol{R}_{\hat{X}X} + 2\boldsymbol{R}_{X\hat{X}} \boldsymbol{D}_\mu^2 \boldsymbol{R}_{\hat{X}X} + Tr(\boldsymbol{D}_\mu^2 \boldsymbol{R}_{XX}) \boldsymbol{R}_{\hat{X}\hat{X}}$. Therefore, the stability in the mean-square sense must be ensured by letting all eigenvalues of $\boldsymbol{GFG}$ satisfy

$$| \lambda\{\boldsymbol{GFG}\} | < 1. \tag{24}$$

The term $\boldsymbol{F}$ contains the space-time data statistics while $\boldsymbol{G}$ represents the topology. We conclude that under the same simulation settings (a fixed value of $\boldsymbol{F}$), the diffusion strategy has a stabilizing effect on the network in the mean-square sense. If $\boldsymbol{G} = \boldsymbol{I}$, the algorithm reduces to the decentralized control. From (24) it can be seen that the decentralized control ($\boldsymbol{G} = \boldsymbol{I}$) has a smaller convergence zone compared to the diffusion control ($\boldsymbol{G} \neq \boldsymbol{I}$). In the simulation part, the convergence curves of these two control methods are compared in Fig. 8, which verifies the conclusion we arrived here.

3.2.3 Steady-state EMSE and ANC network design procedure

We now examine the estimation accuracy after the cooperative learning process reaches steady state. The global and local node steady-state EMSEs are defined as

$$J = \tfrac{1}{K} Tr(\boldsymbol{R}_{xx} \boldsymbol{\Xi}(\infty)) \tag{25a}$$

$$J_k = Tr(\boldsymbol{R}_{xx,k} \boldsymbol{\Xi}_k(\infty)) \tag{25b}$$

where the global and local input covariance matrices are defined as

$$\boldsymbol{R}_{xx} = \mathrm{diag}\{\boldsymbol{R}_{xx,1}, ..., \boldsymbol{R}_{xx,K}\} \text{ and } \boldsymbol{R}_{xx,k} = E[\boldsymbol{x}_k(n) \boldsymbol{x}_k^T(n)].$$

At steady state, (20) reads

$$\begin{aligned} \boldsymbol{\Xi}(\infty) = {} & \boldsymbol{\Xi}_G(\infty) - \boldsymbol{D}_\mu \boldsymbol{R}_{\hat{X}X} \boldsymbol{\Xi}_G(\infty) - \boldsymbol{\Xi}_G(\infty) \boldsymbol{R}_{X\hat{X}} \boldsymbol{D}_\mu \\ & + \boldsymbol{D}_\mu (\boldsymbol{Q}_\Xi(\infty) + \boldsymbol{D}_\Sigma \boldsymbol{R}_{XX}) \boldsymbol{D}_\mu + \boldsymbol{D}_\mu (\widetilde{\boldsymbol{R}}_\psi + \widetilde{\sigma}_\psi^2 \boldsymbol{R}_{\hat{X}\hat{X}}) \boldsymbol{D}_\mu. \end{aligned} \tag{26}$$

Multiplying (26) with an arbitrary matrix Σ and taking trace of it, we get

$$\begin{aligned} Tr(\Sigma \boldsymbol{\Xi}(\infty)) = {} & Tr(\boldsymbol{G}\Sigma\boldsymbol{G}\boldsymbol{\Xi}(\infty)) - Tr(\boldsymbol{G}\Sigma\boldsymbol{D}_\mu \boldsymbol{R}_{\hat{X}X} \boldsymbol{G}\boldsymbol{\Xi}(\infty)) - Tr(\boldsymbol{G}\boldsymbol{\Xi}(\infty)\boldsymbol{G}\boldsymbol{R}_{X\hat{X}} \boldsymbol{D}_\mu \Sigma) \\ & + Tr(\boldsymbol{D}_\mu \Sigma \boldsymbol{D}_\mu \boldsymbol{Q}_\Xi(\infty)) + Tr(\boldsymbol{D}_\mu \Sigma \boldsymbol{D}_\mu (\widetilde{\boldsymbol{R}}_\psi + \widetilde{\sigma}_\psi^2 \boldsymbol{R}_{\hat{X}\hat{X}})) + Tr(\boldsymbol{D}_\mu \Sigma \boldsymbol{D}_\mu \boldsymbol{D}_\Sigma \boldsymbol{R}_{XX}). \end{aligned} \tag{27}$$

Since it is free to select Σ, we thus can evaluate the steady-state EMSE of the network.

Next, we introduce the vector notation and apply the following properties of the vec operator for some arbitrary matrices $\boldsymbol{A}$ and $\boldsymbol{B}$ to the quantities in (27)

$$\text{vec}(\boldsymbol{A}\Sigma\boldsymbol{B}) = (\boldsymbol{B}\otimes\boldsymbol{A}^T)\text{vec}(\Sigma),\ Tr(\boldsymbol{AB}) = \text{vec}(\boldsymbol{A}^T)^T\text{vec}(\boldsymbol{B}).$$

Using these properties and applying the vec operator to $\boldsymbol{\Xi}(\infty)$ and Σ, i.e. $\nu_\Xi = \text{vec}(\boldsymbol{\Xi}(\infty))$ and $\nu_\Sigma = \text{vec}(\Sigma)$, we get the following expression from (27)

$$\begin{aligned}\nu_\Xi^T\nu_\Sigma = {} & \nu_\Xi^T(\boldsymbol{G}\otimes\boldsymbol{G})\nu_\Sigma - \nu_\Xi^T[(\boldsymbol{G}\otimes\boldsymbol{G})(\boldsymbol{I}_{NL}\otimes\boldsymbol{D}_\mu\boldsymbol{R}_{\hat{X}X}) + (\boldsymbol{G}\otimes\boldsymbol{G})^T(\boldsymbol{R}_{X\hat{X}}\boldsymbol{D}_\mu\otimes\boldsymbol{I}_{NL})]\nu_\Sigma \\ & + \nu_\Xi^T(\boldsymbol{G}\otimes\boldsymbol{G})\Theta(\boldsymbol{D}_\mu\otimes\boldsymbol{D}_\mu)\nu_\Sigma + KJ\nu_R^T\nu_\Sigma + \nu_M^T\nu_\Sigma\end{aligned} \tag{28}$$

where the following notations have been defined as

$$\Theta = 2\boldsymbol{R}_{X\hat{X}}\otimes\boldsymbol{R}_{\hat{X}X} \tag{29}$$

$$\nu_M = (\boldsymbol{D}_\mu\otimes\boldsymbol{D}_\mu)^T[\text{vec}(\widetilde{\boldsymbol{R}}_\psi + \widetilde{\sigma}_\psi^2\boldsymbol{R}_{\hat{X}\hat{X}}) + \text{vec}(\boldsymbol{D}_\Sigma\boldsymbol{R}_{XX})] \tag{30}$$

$$\nu_R = (\boldsymbol{G}\otimes\boldsymbol{G})(\boldsymbol{D}_\mu\otimes\boldsymbol{D}_\mu)\text{vec}(\boldsymbol{R}_{\hat{X}\hat{X}}). \tag{31}$$

Eq. (30) is the driving vector that contains the driving terms.

After some simple algebraic operations, (28) becomes

$$\nu_\Xi^T\overline{\boldsymbol{F}}\nu_\Sigma = KJ\nu_R^T\nu_\Sigma + \nu_M^T\nu_\Sigma \tag{32}$$

where $\overline{\boldsymbol{F}} = \boldsymbol{I}_{L^2K^2} - (\boldsymbol{G}\otimes\boldsymbol{G})[\boldsymbol{I}_{L^2K^2} - (\boldsymbol{I}_{NL}\otimes\boldsymbol{D}_\mu\boldsymbol{R}_{\hat{X}X}) - (\boldsymbol{R}_{X\hat{X}}\boldsymbol{D}_\mu\otimes\boldsymbol{I}_{NL}) + \Theta(\boldsymbol{D}_\mu\otimes\boldsymbol{D}_\mu)]$.

Consider the possibility $\nu_\Sigma = \overline{\boldsymbol{F}}^{-1}\text{vec}(\boldsymbol{R}_{xx})$. This leads to the global steady-state EMSE over the network

$$J = \tfrac{1}{K}\nu_M^T\overline{\boldsymbol{F}}^{-1}\text{vec}(\boldsymbol{R}_{xx})/[1-\nu_R^T\overline{\boldsymbol{F}}^{-1}\text{vec}(\boldsymbol{R}_{xx})]. \tag{33}$$

Similarly, the steady-state EMSE for each node becomes

$$J_k = \nu_M^T\overline{\boldsymbol{F}}^{-1}\text{vec}(\breve{\boldsymbol{R}}_{xx,k})/[1-\nu_R^T\overline{\boldsymbol{F}}^{-1}\text{vec}(\breve{\boldsymbol{R}}_{xx,k})] \tag{34}$$

where $\breve{\boldsymbol{R}}_{xx,k}$ is a block diagonal matrix of the same size as $\boldsymbol{R}_{xx}$ and all the block elements on the diagonal are null except the kth one $\boldsymbol{R}_{xx,k}$.

TABLE I COMPARISON OF THE EXPERIMENTAL AND PREDICTED GLOBAL STEADY-STATE EMSE (dB/20μPA)

r	0		0.05		0.1	
μ	0.01	0.002	0.01	0.002	0.01	0.002
Simu	-22.8	-31.0	-20.8	-30.4	-18.4	-27.9
Theo	-23.1	-31.4	-21.3	-30.8	-19.3	-28.7
Δ	0.3	0.4	0.5	0.4	0.9	0.8

TABLE II PROPOSED DESIGN PROCEDURE FOR NETWORKED ANC SYSTEMS

Given the desired steady-state EMSE for the ANC controller, ξ, as well as the prior knowledge or estimate of the input power and noise variance.

Step 1 Calculate the step-size of the ANC controller μ from (35) using the small step size approximation:

$$\mu \approx [K\xi + \sqrt{(K\xi)^2 - 4r_1 r_2}]/2r_1,$$

where r_1 and r_2 have been defined in (35). To calculate the parameters, refer to the statistics defined in the following equations:

$\boldsymbol{D}_\Sigma$	(19)
$\boldsymbol{R}_{\hat{X}X}$, $\boldsymbol{\psi}_\infty$	(7)
$\boldsymbol{R}_{XX}$, $\boldsymbol{R}_{\hat{X}\hat{X}}$	(18)

Step 2 Check the stability conditions for the ANC controller in (13) and (24). If these conditions are violated, a smaller ξ should be chosen.

The global steady-state EMSEs (33) are compared with the simulation results in Table I. Different step-sizes and radius values are examined. The settings are identical to those in Fig. 5. It can be seen that the prediction deviation is within 1 dB in all the cases tested. The deviation generally increases with the radius *r*.

Next, a design procedure for networked ANC systems is derived from the theoretical analysis. Given the prior knowledge on the power of the input, and the variance of background noise, we shall determine the step-sizes for the ANC controllers in order to achieve a desired global steady-state EMSE ξ. Assuming all controllers use the same step-size and according to Appendix B, the step-size can be approximately chosen as

$$\mu \approx [K\xi + \sqrt{(K\xi)^2 - 4r_1 r_2}]/2r_1 \tag{35}$$

where $r_1 = \mathrm{vec}(\boldsymbol{D}_\Sigma \boldsymbol{R}_{XX})[\boldsymbol{R}_\Sigma^{-1} - \frac{1}{trace(\boldsymbol{I}_G \boldsymbol{R}_\Sigma^{-1})}\boldsymbol{R}_\Sigma^{-1}\boldsymbol{I}_G\boldsymbol{R}_\Sigma^{-1}]\mathrm{vec}(\boldsymbol{R}_{xx})$, with $\boldsymbol{I}_G = \boldsymbol{I}_{L^2K^2} - (\boldsymbol{G}\otimes\boldsymbol{G})\boldsymbol{I}_{L^2K^2}$ and $\boldsymbol{R}_\Sigma = (\boldsymbol{G}\otimes\boldsymbol{G})(\boldsymbol{I}_{NL}\otimes\boldsymbol{R}_{\hat{X}X} + \boldsymbol{R}_{X\hat{X}}\otimes\boldsymbol{I}_{NL})$, is related to noise variance and input covariance matrices and $r_2 = [\mathrm{vec}(\widetilde{\boldsymbol{R}}_{\psi 0} + \widetilde{\sigma}_{\psi 0}^2 \boldsymbol{R}_{\hat{X}\hat{X}})][\boldsymbol{R}_\Sigma^{-1} - \frac{1}{trace(\boldsymbol{I}_G \boldsymbol{R}_\Sigma^{-1})}\boldsymbol{R}_\Sigma^{-1}\boldsymbol{I}_G\boldsymbol{R}_\Sigma^{-1}]\mathrm{vec}(\boldsymbol{R}_{xx})$ is determined by the network topology terms $\widetilde{\boldsymbol{R}}_{\psi 0} = (\boldsymbol{I}_{LK} - \boldsymbol{G})\boldsymbol{\psi}_\infty\boldsymbol{\psi}_\infty^T(\boldsymbol{I}_{LK} - \boldsymbol{G})^T$ and $\widetilde{\sigma}_{\psi 0}^2 = Tr(\boldsymbol{R}_{XX}^{-1}\widetilde{\boldsymbol{R}}_{\psi 0})$. Note, the desired EMSE ξ is bounded by a minimum value $2\sqrt{r_1 r_2}$. The proposed design procedure is summarized in Table II. It can be seen that if the combination matrix is chosen as the identity matrix, $r_2 = 0$ and the step-size selection rule is similar to that of the conventional FxLMS algorithm [24][30].

The effectiveness of the proposed procedure in Table II is verified by a design example. The settings are identical to those in Fig. 5 and the radius is set to a medium value r = 0.05. The desired steady-state global EMSE for the ANC controller is -20 dB. According to Table II, the step-size is to be calculated by using the estimated or known noise power and input covariance matrices.

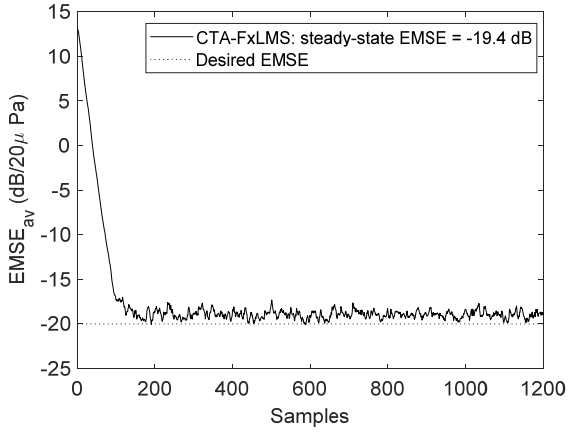

Fig. 6. Learning curves of the global EMSE and comparison with the desired value.

The details are as follows: 1) formulate the noise matrix $\boldsymbol{D}_{\Sigma}$ according to (19); 2) formulate the covariance matrices, such as $\boldsymbol{R}_{\hat{X}X}$, $\boldsymbol{R}_{XX}$, and $\boldsymbol{R}_{\hat{X}\hat{X}}$; 3) use the noise and input covariance matrices to calculate factors r_1 and r_2 as shown in (35); 4) obtain the step-size from $\mu \approx [K\xi + \sqrt{(K\xi)^2 - 4r_1 r_2}]/2r_1$, which turns out to be 0.009 (Step 1 in Table II); 5) apply the step-size to (13) and (24) to see whether the stability conditions are satisfied (Step 2 in Table II). Using the calculated step-size, the obtained steady-state EMSE for the ANC controller is -19.4 dB, which is very close to the desired value as shown in Fig. 6. This shows that the approximations made in Table II are reasonable and illustrates the effectiveness of the proposed design procedure for networked ANC systems.

4. Simulation Results

In this section, we compare different control strategies and study a 10-node ANC network for noise control in open areas. In the case study, the effect of the network layout strategies on noise control is examined. Based on the performance analysis, the proposed design method for ANC networks is tested.

The following simulations are based on a multi-channel ANC system as shown in Fig. 1, and we only

discuss a system with offline secondary-path modeling. The online modeling for secondary paths [31] can be extended to the multi-channel system in a similar way as in [24]. In experiment 1, different control strategies are compared in the multi-channel ANC system. Experiment 2 studies the transform loss (TL) of the ANC network. In experiment 3, a 10-node ANC network is considered. The effect of network topology on the noise control performance is evaluated. In experiment 4, the proposed ANC network design strategy is tested. We use a Metropolis weight matrix [21] as the combining matrix in all experiments of this paper and all simulation results are averaged over 100 Monte Carlo runs if not specified.

4.1 Comparison of different control strategies

In this experiment, the control strategies under test include the centralized, decentralized, incrementally distributed, and diffusion control methods. We consider an ANC system with 10 channels, i.e. the network has 10 pairs of loudspeakers and microphones. The primary path is measured experimentally and the measured room impulse response (RIR) is shown in Fig. 7.

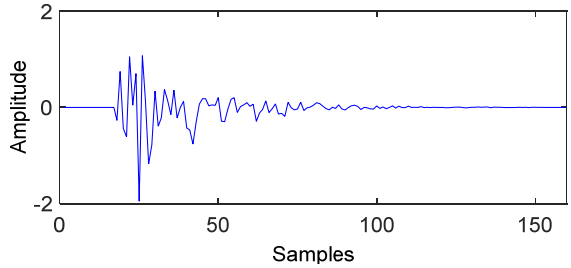

Fig. 7. The measured RIR for the primary paths $\boldsymbol{p}_0$. $L = 160$. The unit of the amplitude is Pa.

Suppose the ANC system aims to cancel out the low frequency noise, say under 500 Hz and the sampling rate is 1 KHz. The RIR, say $\boldsymbol{p}_0$, has a length of 160 (the reverberation time is about hundreds of milliseconds). The adaptive filter for the controller has the same length. The secondary paths have a length of 10 and they are estimated offline with a small bias. The SNR is set to 20 dB.

In the first test, a small radius is used, which is set to $r = 0.01$ and the step-sizes for the controllers are chosen as $\mu = 0.001$. The simulation results for the global EMSE learning curves are shown in Fig. 8(a). It can be seen that the incremental control method has a higher steady-state residual noise level while the decentralized control method increases the EMSE value gradually as the iteration. The diffusion control has a

similar performance as the well-performed centralized control. Next, the radius increases to $r = 0.07$ and the step-size is set to $\mu = 0.0003$. In this case, the decentralized control method diverges while the incremental control method has a higher residual noise level. The centralized and diffusion control methods still have the best performance of all algorithms under comparison. Considering the computational cost of different control methods as shown in Table III, the diffusion control saves the arithmetic complexity by one order. Therefore, it is more appropriate for practical use.

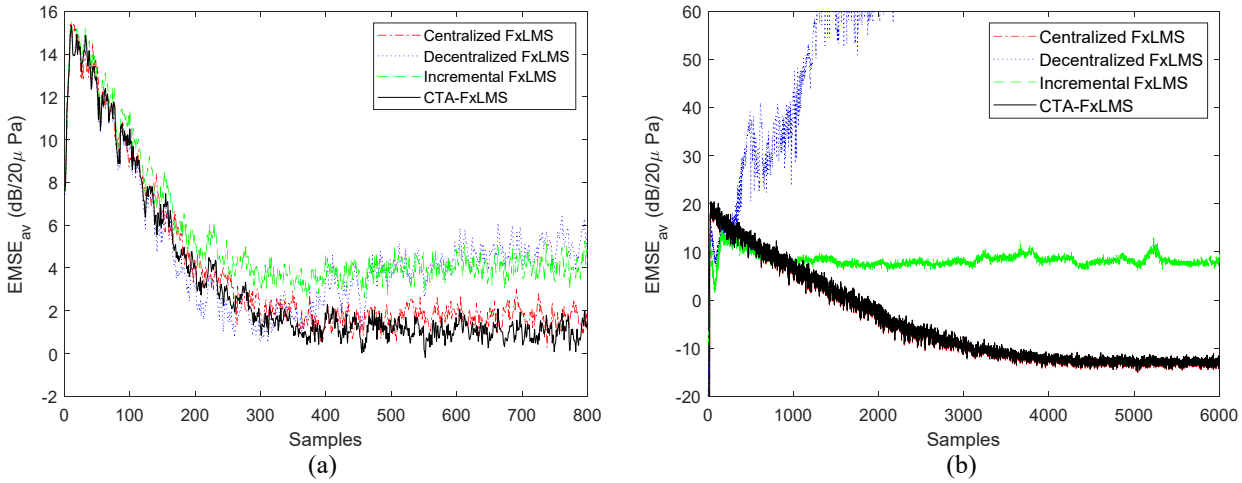

Fig. 8. Global EMSE learning curves with different control strategies for the ANC controller: (a) $\mu = 0.001$, $r = 0.01$; (b) $\mu = 0.0003$, $r = 0.07$; $L = 160$, $K = 10$.

TABLE III ARITHMETIC COMPLEXITIES OF VARIOUS CONTROL METHODS

	Centralized FxLMS	Decentralized FxLMS	Distributed FxLMS
Secondary path modeling	K^2	K	K
Adaptive filter	K^2L	KL	KL

4.2 Performance of ANC networks with different number of nodes

In this experiment, the performance of ANC networks is measured by the noise attenuation over all nodes. We define the TL for ANC networks by the noise reduction averaged at all nodes. The formulation is described as

$$TL_{net} = 10\log_{10}\frac{1}{K}\frac{\sum_{k=1}^{K}\overline{d_k^2}(n)}{\sum_{k=1}^{K}\overline{e_k^2}(n)} \tag{36}$$

where the unwanted noise $d_k(n)$ and the ANC network residual signals $e_k(n)$ have been defined,

respectively, in (2) and (1).

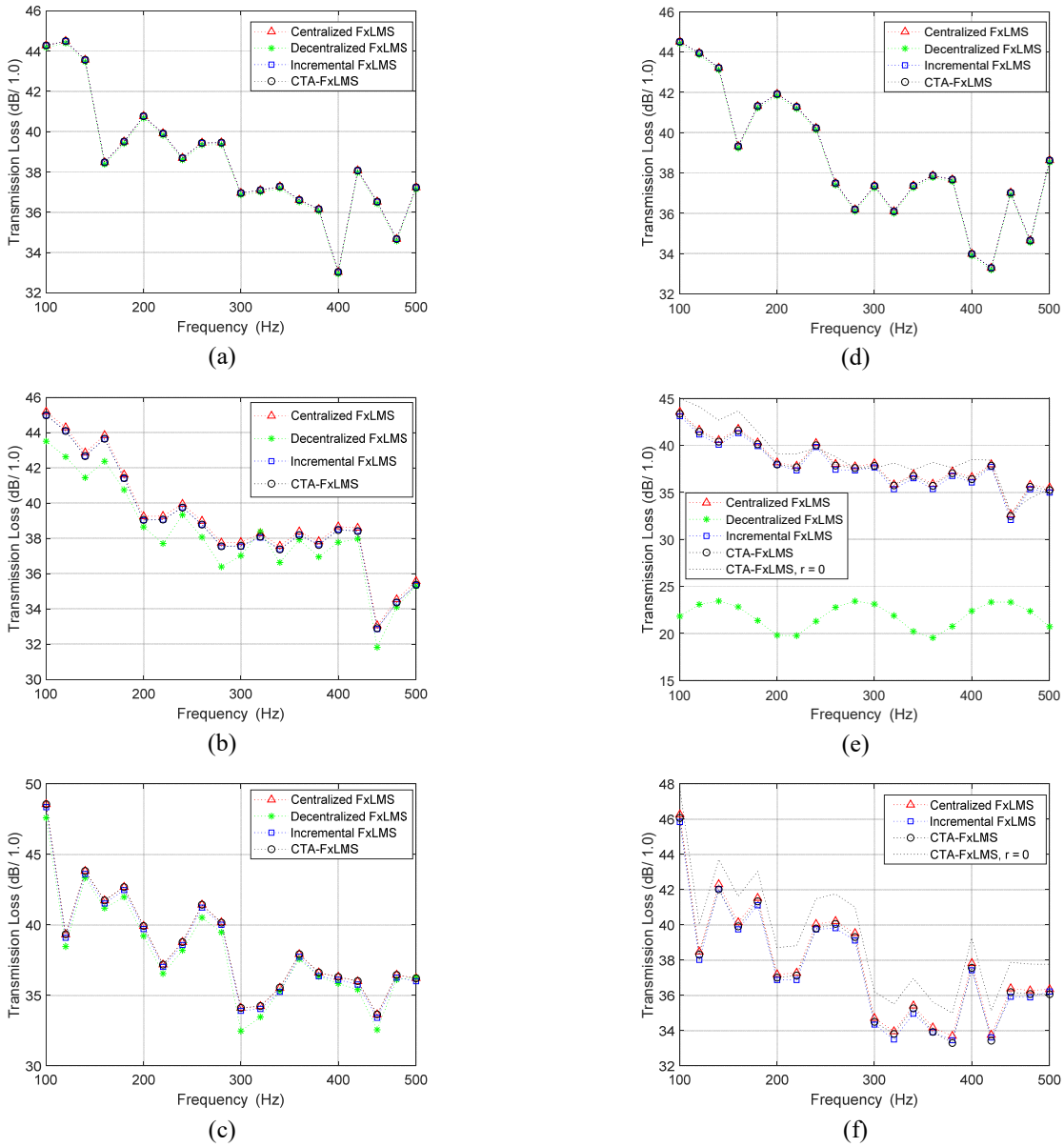

Fig. 9. TL for ANC networks with different number of nodes $K = 1$ [in (a) and (d)], $K = 5$ [in (b) and (e)], $K = 10$ [in (c) and (f)]; and radius $r = 0$ [in (a)-(c)], $r = 0.1$ [in (d)-(f)]. The step-size $\mu = 0.0005$.

Different number of nodes has been used in the ANC network, with or without radius deviation. The step-size is set to 0.0005. The radius is set to $r = 0$ and 0.1. The number of nodes considered is $K = 1$, 5 and 10. The other settings are identical to those in the previous experiment. The simulation results of TL for different control strategies aforementioned are shown in Fig. 9. It can be seen that when the number of nodes is 1 [Figs. 9(a) and (d)], the simulation results from all strategies are identical (the seeds are fixed when generating

random sequences used in the experiments). Generally, the TL decreases with frequency from 100 Hz to 500 Hz. When $K = 5$ and $r = 0$ [Fig. 9(b)], the decentralized control method shows lower TL values at most of the frequency bins compared with other control strategies. This result is consistent with the convergence curves as shown in Fig. 8(a), where the decentralized control method has higher steady-state EMSE. The overall TL performance is similar to that for $K = 1$. As K increases to 10 [Fig. 9(c)], the decentralized control method has lower TL than that for $K = 5$. The overall performance shows fluctuation at different frequency bins. It means the increased number of nodes could enlarge the noise control area at the cost of the degraded performance at certain frequency bins. When the radius increases to 0.1, similar results can be observed in Figs. 9(e) and (f) except that the decentralized control method diverges. The calculated results for conventional decentralized control are not reliable or the TL calculated is less than 0.

4.3 A 10-node ANC network case study

In this experiment, we examine the effect of the node (a pair of loudspeaker and error sensor) positions on the control performance and study a specific case of ANC network. Testing is performed using a 10-node network as in the previous experiment. The RIRs for both primary and secondary paths are simplified, i.e. the primary paths have a length of 10 and the secondary paths have a length of 3. The step-size is set to 0.01. The other settings are identical to those in the previous experiment if not specified.

TABLE IV NOISE REDUCTIONS AT ERROR SENSORS: $r = 0$ (dB/20μ Pa)

Node No.	1	2	3	4	5	6	7	8	9	10
Before ANC	13.9	13.9	13.9	13.9	13.9	13.9	13.9	13.9	13.9	13.9
After ANC	-5.8	-6.0	-6.0	-6.0	-5.8	-5.9	-6.0	-6.0	-5.8	-5.7
Noise Reduction	19.7	19.9	19.9	19.9	19.7	19.8	19.9	19.9	19.7	19.6

TABLE V NOISE REDUCTIONS AT ERROR SENSORS: $r = 0.05$ (dB/20μ Pa)

Node No.	1	2	3	4	5	6	7	8	9	10
Before ANC	13.9	13.5	13.5	13.3	13.5	13.6	13.5	13.3	13.1	13.0
After ANC	-2.8	-2.2	-5.7	-5.2	-4.0	-3.6	-4.6	-6.3	-4.0	-3.6
Noise Reduction	16.7	15.7	19.2	18.5	17.4	17.2	18.1	19.7	17.1	16.6

TABLE VI NOISE REDUCTIONS AT ERROR SENSORS: $r = 0.1$ (dB/20μ Pa)

Node No.	1	2	3	4	5	6	7	8	9	10
Before ANC	13.9	13.2	13.2	12.9	13.4	13.8	13.6	13.0	12.6	12.5
After ANC	1.2	2.3	-4.2	-2.6	-0.6	0.2	-1.5	-6.0	-0.4	0.1
Noise Reduction	12.7	10.9	17.4	15.5	14.0	13.6	15.1	19.0	13.0	12.4

The noise levels at the error sensors before and after implementing ANC under the setting of r = 0, 0.05, and 0.1 have been listed, respectively, in Tables IV, V, and VI. In Table IV, noise reduction at each node has a similar value. However, the deviation of noise reduction at each node increases as the radius (see Tables V and VI). The highest noise reduction in each table (marked in grey) is similar; while the smallest value (marked in underline) decreases as the radius. The smallest noise reduction is observed at node 2, which connects to 5 other nodes as shown in Fig. 10. The main reason for the decreased noise reduction is that the distribution strategy introduces an estimation bias, as shown in (7), (8), and (10), and some of the nodes do not converge to the Weiner solutions. Although distribution introduces bias to each node, the overall performance of the ANC network is not affected as shown in Fig. 8. On the other hand, this distribution strategy decreases computational burden significantly, which is suitable to be implemented on hardware for practical use.

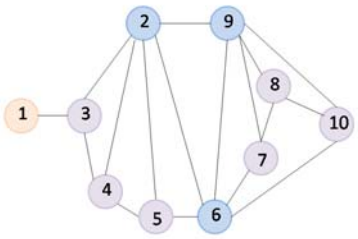

Fig. 10. A 10-nod network topology.

The noise spectra at Node 2 and 8 (respectively, corresponding to the smallest and largest noise reduction) before and after implementing ANC are shown in Fig. 11. The configurations are r = 0.05 and 0.1 It can be seen from Fig. 11(a) that the noise levels at these two nodes have been reduced almost to the background noise levels (SNR is set to 20 dB) when the radius is set to a medium value. Fig. 11(b) provides evidence that when the radius further increases, the optimal location (Node 8 in this case) remains satisfactory performance while some nodes may have a reduction less than 5 dB at a certain frequency (e.g. Node 2 at around 330 Hz). The simulation results at other nodes are presented in Appendix C to show the efficiency of diffusion control in noise reduction.

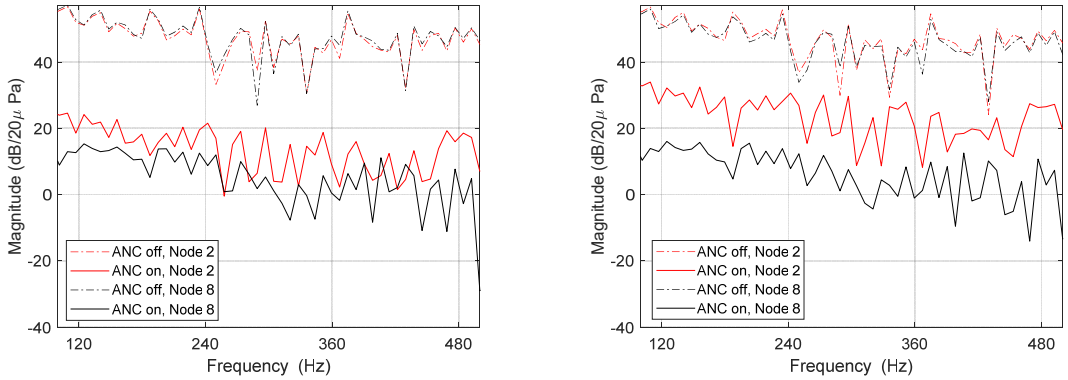

Fig. 11. Noise levels at the network nodes before and after switching on the ANC system (a) $r = 0.05$, and (b) $r = 0.1$.

5. Conclusion

To better understand the mechanism of diffusion ANC systems, the performance of Diff-FxLMS based ANC systems has been analyzed. New difference equations describing the mean and mean squares convergence behaviors of such ANC networks have been derived. Based on these difference equations, the stability of the system is analyzed and the steady-state EMSEs for the ANC controller are obtained. The analyses provide useful insight as well as guidance for the design of ANC networks, which are illustrated by a design example. The simulation results are found to be in good agreement with the theoretical predictions. A specific case of a 10-node ANC network has been studied in detail in terms of TL and noise topology.

Acknowledgment

The work described in this study was supported by a grant from the Hong Kong Polytechnic University (The Hong Kong Polytechnic University Postdoctoral Fellowships Scheme, G-YW0L), National Natural Science Foundation of China (61901174), Guangdong Basic and Applied Basic Research Foundation (2019A1515010771), and Open Projects Fund of Key Laboratory of Ecology and Energy-saving Study of Dense Habitat (Tongji University), Ministry of Education (2019030105).

Appendix A: Derivation of Mean Squares Difference Equation

In this appendix, we first evaluate (17) and then rewrite (16) to a concise form.

According to (17), $\boldsymbol{Q}(n)$ can be written as a summation of several weight error correlation matrices defined as

$$\hat{\boldsymbol{\Xi}}_G(n) = E[\hat{\boldsymbol{v}}_G(n)\hat{\boldsymbol{v}}_G^T(n)] = \boldsymbol{G}\Delta\boldsymbol{\psi}\Delta\boldsymbol{\psi}^T\boldsymbol{G} + \boldsymbol{\Xi}_G(n) + \bar{\boldsymbol{v}}_G(n)\Delta\boldsymbol{\psi}^T\boldsymbol{G} + \boldsymbol{G}\Delta\boldsymbol{\psi}\bar{\boldsymbol{v}}_G^T(n)$$

$$\boldsymbol{\Xi}_{\Sigma,G}(n) = \bar{\boldsymbol{v}}_G(n)\Delta\boldsymbol{\psi}^T\boldsymbol{G} + \boldsymbol{G}^T\Delta\boldsymbol{\psi}\bar{\boldsymbol{v}}_G^T(n)$$

where $\hat{\boldsymbol{v}}(n) = \boldsymbol{\psi}_0 - \boldsymbol{\psi}_C(n)$ and $\hat{\boldsymbol{v}}_G(n) = \boldsymbol{G}\hat{\boldsymbol{v}}(n)$. Using the above notations, Eq. (17) can be described as

$$\boldsymbol{Q}(n) = \boldsymbol{Q}_{\Xi}(n) + \boldsymbol{Q}_0(n) + \boldsymbol{Q}_1(n) + \boldsymbol{Q}_2(n) \tag{A.1}$$

where $\boldsymbol{Q}_{\Xi}(n) = E[\hat{\boldsymbol{\mathcal{X}}}(n)\boldsymbol{\mathcal{X}}^T(n)\hat{\boldsymbol{\Xi}}_G(n)\boldsymbol{\mathcal{X}}(n)\hat{\boldsymbol{\mathcal{X}}}^T(n)]$, $\boldsymbol{Q}_0(n) = E[\hat{\boldsymbol{\mathcal{X}}}(n)\boldsymbol{\mathcal{X}}^T(n)\boldsymbol{G}\Delta\boldsymbol{\psi}\Delta\boldsymbol{\psi}^T\boldsymbol{G}\boldsymbol{\mathcal{X}}(n)\hat{\boldsymbol{\mathcal{X}}}^T(n)]$, $\boldsymbol{Q}_1(n) = E[\hat{\boldsymbol{\mathcal{X}}}(n)\boldsymbol{\mathcal{X}}^T(n)\boldsymbol{\Xi}_{\Sigma,G}(n)\boldsymbol{\mathcal{X}}(n)\hat{\boldsymbol{\mathcal{X}}}^T(n)]$ and $\boldsymbol{Q}_2(n) = E[\hat{\boldsymbol{\mathcal{X}}}(n)\boldsymbol{\eta}_{\Sigma}(n)\boldsymbol{\eta}_{\Sigma}^T(n)\hat{\boldsymbol{\mathcal{X}}}^T(n)]$.

By using the Gaussian factoring theorem [32] and after some manipulations, $\boldsymbol{Q}_{\Xi}(n)$ can be written as

$$\boldsymbol{Q}_{\Xi}(n) = 2\boldsymbol{R}_{\hat{X}X}\boldsymbol{\Xi}_G(n)\boldsymbol{R}_{X\hat{X}} + \boldsymbol{R}_{\hat{X}\hat{X}}Tr(\boldsymbol{\Xi}_G(n)\boldsymbol{R}_{XX}) \tag{A.2}$$

where $\boldsymbol{R}_{XX} = E[\boldsymbol{\mathcal{X}}(n)\boldsymbol{\mathcal{P}}(n)\boldsymbol{\mathcal{X}}^T(n)]$. $\boldsymbol{Q}_0(n)$ and $\boldsymbol{Q}_1(n)$ can be simplified in a similar way.

The diagonal matrix of the noise variance can be expressed as

$$\boldsymbol{D}_{\Sigma} = \mathrm{diag}\{\sigma_{\Sigma,1}^2\boldsymbol{I}_L,...,\sigma_{\Sigma,K}^2\boldsymbol{I}_L\} \tag{A.3}$$

such that $\boldsymbol{Q}_2(n) = \boldsymbol{D}_{\Sigma}\hat{\boldsymbol{R}}_{XX}$.

Substituting (A.1)-(A.3) into (16), we find

$$\begin{aligned}\boldsymbol{\Xi}(n+1) = {} & \boldsymbol{\Xi}_G(n) - \boldsymbol{D}_{\mu}\boldsymbol{R}_{\hat{X}X}\boldsymbol{\Xi}_G(n) - \boldsymbol{\Xi}_G(n)\boldsymbol{R}_{X\hat{X}}\boldsymbol{D}_{\mu} + \boldsymbol{D}_{\mu}(\boldsymbol{Q}_{\Xi}(n) + \boldsymbol{D}_{\Sigma}\boldsymbol{R}_{XX})\boldsymbol{D}_{\mu} \\ & + \boldsymbol{D}_{\mu}(\widetilde{\boldsymbol{R}}_{\psi} + \widetilde{\sigma}_{\psi}^2\boldsymbol{R}_{\hat{X}\hat{X}})\boldsymbol{D}_{\mu} + \boldsymbol{D}_{\mu}[\boldsymbol{R}_{\hat{X}X}\boldsymbol{\Xi}_{\Sigma,G}(n)\boldsymbol{R}_{X\hat{X}} + Tr(\boldsymbol{\Xi}_{\Sigma,G}(n)\boldsymbol{R}_{XX})\boldsymbol{R}_{\hat{X}\hat{X}}]\boldsymbol{D}_{\mu}\end{aligned} \tag{A.4}$$

where $\widetilde{\sigma}_{\psi}^2 = Tr(\boldsymbol{R}_{XX}^{-1}\widetilde{\boldsymbol{R}}_{\psi})$.

Appendix B: Derivation of Step-Size Selection Formula

In this appendix, we calculate a step-size such that the steady-state EMSE meets the design requirement ξ. First, we assume that all controllers use the same step-size. Secondly, the step-size is assumed to be small compared to the input power such that the denominator of (33) can be omitted.

Under these assumptions and applying the lemma $(\boldsymbol{A}+\boldsymbol{B})^{-1} = \boldsymbol{A}^{-1} - \frac{1}{1+g}\boldsymbol{A}^{-1}\boldsymbol{B}\boldsymbol{A}^{-1}$, where $g = trace(\boldsymbol{B}\boldsymbol{A}^{-1})$, the term $\overline{\boldsymbol{F}}^{-1}$ can be written as

$$\overline{\boldsymbol{F}}^{-1} \approx \boldsymbol{I}_G + \mu\boldsymbol{R}_\Sigma = \tfrac{1}{\mu}[\boldsymbol{R}_\Sigma^{-1} - \tfrac{1}{\mu+trace(\boldsymbol{I}_G\boldsymbol{R}_\Sigma^{-1})}\boldsymbol{R}_\Sigma^{-1}\boldsymbol{I}_G\boldsymbol{R}_\Sigma^{-1}] \tag{B.1}$$

where $\boldsymbol{I}_G = \boldsymbol{I}_{L^2K^2} - (\boldsymbol{G}\otimes\boldsymbol{G})\boldsymbol{I}_{L^2K^2}$ and $\boldsymbol{R}_\Sigma = (\boldsymbol{G}\otimes\boldsymbol{G})(\boldsymbol{I}_{NL}\otimes\boldsymbol{R}_{\hat{X}X} + \boldsymbol{R}_{X\hat{X}}\otimes\boldsymbol{I}_{NL})$. Substituting (B.1) to (33), we have

$$\begin{aligned} J &\approx \tfrac{1}{K}\mu[\mathrm{vec}(\widetilde{\boldsymbol{R}}_\psi + \widetilde{\sigma}_\psi^2\boldsymbol{R}_{\hat{X}\hat{X}}) + \mathrm{vec}(\boldsymbol{D}_\Sigma\boldsymbol{R}_{XX})][\boldsymbol{R}_\Sigma^{-1} - \tfrac{1}{trace(\boldsymbol{I}_G\boldsymbol{R}_\Sigma^{-1})}\boldsymbol{R}_\Sigma^{-1}\boldsymbol{I}_G\boldsymbol{R}_\Sigma^{-1}]\mathrm{vec}(\boldsymbol{R}_{xx}) \\ &= \tfrac{1}{K}(\tfrac{1}{\mu}r_2 + \mu r_1) \end{aligned} \tag{B.2}$$

where $r_1 = \mathrm{vec}(\boldsymbol{D}_\Sigma\boldsymbol{R}_{XX})[\boldsymbol{R}_\Sigma^{-1} - \tfrac{1}{trace(\boldsymbol{I}_G\boldsymbol{R}_\Sigma^{-1})}\boldsymbol{R}_\Sigma^{-1}\boldsymbol{I}_G\boldsymbol{R}_\Sigma^{-1}]\mathrm{vec}(\boldsymbol{R}_{xx})$ is related to noise variance and input covariance matrix and $r_2 = [\mathrm{vec}(\widetilde{\boldsymbol{R}}_{\psi 0} + \widetilde{\sigma}_{\psi 0}^2\boldsymbol{R}_{\hat{X}\hat{X}})][\boldsymbol{R}_\Sigma^{-1} - \tfrac{1}{trace(\boldsymbol{I}_G\boldsymbol{R}_\Sigma^{-1})}\boldsymbol{R}_\Sigma^{-1}\boldsymbol{I}_G\boldsymbol{R}_\Sigma^{-1}]\mathrm{vec}(\boldsymbol{R}_{xx})$ is determined by the network topology terms $\widetilde{\boldsymbol{R}}_{\psi 0} = (\boldsymbol{I}_{LK} - \boldsymbol{G})\boldsymbol{\psi}_\infty\boldsymbol{\psi}_\infty^T(\boldsymbol{I}_{LK} - \boldsymbol{G})^T$ and $\widetilde{\sigma}_{\psi 0}^2 = Tr(\boldsymbol{R}_{XX}^{-1}\widetilde{\boldsymbol{R}}_{\psi 0})$. Given the prior on input signal and the required steady-state EMSE ξ, the step-size can be approximately chosen as

$$\mu \approx [K\xi + \sqrt{(K\xi)^2 - 4r_1r_2}]/2r_1 \tag{B.3}$$

given that $K\xi \geq 2\sqrt{r_1r_2}$.

Appendix C: Noise Reduction Performance

Simulation is conducted under the same settings as those in Fig. 11. The noise levels at the other 8 nodes are shown in Fig. A. Similar performance at each node can be observed, which shows the efficiency of diffusion control in noise reduction over the extended area.

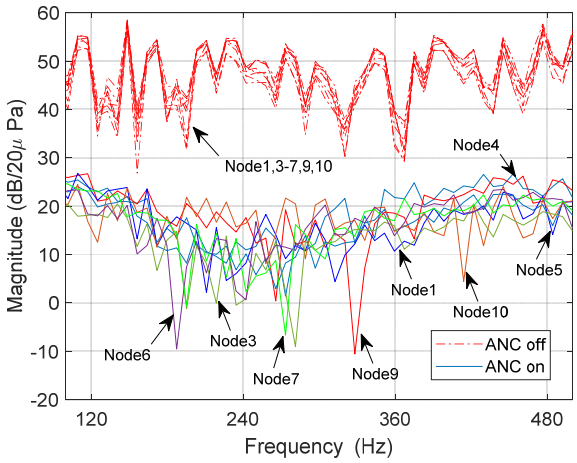

Fig. A. Noise levels at the other nodes before and after switching on the ANC system, $r = 0.1$.

References

[1] S. Elliott, I. Stothers, P. Nelson, A multiple error LMS algorithm and its application to the active control of sound and vibration, *IEEE Trans. Speech Signal Process.*, 35 (1987) 1423–1434. https://doi.org/ 10.1109/TASSP.1987.1165044

[2] S. Elliott, J. Cheer, B. Lam, C. Shi, W. S. Gan, A wavenumber approach to analysing the active control of plane waves with arrays of secondary sources, *J. Sound Vib*. 419 (2018) 405–419. https://doi.org/10.1016/j.jsv.2018.01.028

[3] K. Wang, J. Tao, X. Qiu, Boundary control of sound transmission into a cavity through its opening, *J. Sound Vib*. 442 (2019) 350–365. https://doi.org/10.1016/j.jsv.2018.11.006

[4] H. Lou and D. Y. Ou, A comparative field study of indoor environmental quality in two types of open-plan offices: Open-plan administrative offices and open-plan research offices, *Build. Environ.*, 148 (2019), 394–404. https://doi.org/10.1016/j.buildenv.2018.11.022

[5] C. M. Mak, Special issue on building acoustics and noise control, *Build. Environ.*, 94 (2015), 751. https://doi.org/10.1016/j.buildenv.2015.10.011

[6] K. Yin, H. Zhao, L. Lu, Functional link artificial neural network filter based on the q-gradient for nonlinear active noise control, *J. Sound Vib*. 435 (2018) 205–217. https://doi.org/10.1016/j.jsv.2018.08.015

[7] K. Iwai, S. Kinoshita, Y. Kajikawa, Multichannel feedforward active noise control system combined with noise source separation by microphone arrays, *J. Sound Vib*. 453 (2019) 151–173. https://doi.org/10.1016/j.jsv.2019.04.016

[8] D. R. Morgan, An analysis of multiple correlation cancellation loops with a filter in the auxiliary path, *IEEE Trans. Acoust., Speech, Signal Process.*, 28 (1980) 454–67. https://doi.org/10.1109/TASSP.1980.1163430

[9] Y. Li, L. He, C. Shuai, F. Wang, Time-domain filtered-x-Newton narrowband algorithms for active isolation of frequency-fluctuating vibration, *J. Sound Vib*. 367 (2016) 1–21. https://doi.org/10.1016/j.jsv.2015.12.019

[10] L. Wu, X. Qiu, I. S. Burnett, Y. Guo, A recursive least square algorithm for active control of mixed noise, *J. Sound Vib*. 339 (2015) 1–10. https://doi.org/10.1016/j.jsv.2014.11.002

[11] X. L. Tang, C. M. Lee, Time–frequency-domain filtered-x LMS algorithm for active noise control, *J. Sound Vib*. 331 (2012) 5002–5011. https://doi.org/10.1016/j.jsv.2012.07.009

[12] W. S. Levine, *The Control Handbook*, CRC Press, Boca Raton, 1996.

[13] E. Leboucher, P. Micheau, A. Berry, and A. L'Esperance, A stability analysis of a decentralized adaptive feedback active control system of a sinusoidal sound in free space, *J. Acoust. Soc. Am*., 111 (2002) 189–199. https://doi.org/10.1121/1.1427358

[14] L. Zhang, J. Tao, and X. Qiu, Performance analysis of decentralized multi-channel feedback systems for active noise control in free space, *App. Acoust.*, 74 (2013) 181–8. https://doi.org/10.1016/j.apacoust.2012.07.008

[15] G. Zhang, J. Tao, X. Qiu, and I. Burnett, Decentralized two-channel active noise control for single frequency by shaping matrix eigenvalues, *IEEE Trans. Audio, Speech, Lang. Process*., 27 (2019) 44–52. https://doi.org/10.1109/TASLP.2018.2869686

[16] J. A. Mosquera-Sánchez, W. Desmet, L. P. R. de Oliveira, Multichannel feedforward control schemes with coupling compensation for active sound profiling, *J. Sound Vib*. 396 (2017) 1–29. https://doi.org/10.1016/j.jsv.2017.02.016

[17] C. Lopes and A. Sayed, Incremental adaptive strategies over distributed networks, *IEEE Trans. Signal Process*., 55 (2007), 4064–77. https://doi.org/10.1109/TSP.2007.896034

[18] Y. J. Chu and C. M. Mak, Diffusion control for multi-channel ANC systems using filtered-x algorithms, *Pro. 24th Int. Cong. Sound Vib.*, London, UK, 23–27, Jul. 2017.

[19] M. Ferrer, M. Diego, G. Pinero, and A. Gonzalez, Active noise control over adaptive distributed networks, *Signal Process.*, 107 (2015) 82–95. https://doi.org/10.1016/j.sigpro.2014.07.026

[20] A. Sayed, Adaptive Networks, *Pro. IEEE*, 102 (2014), 460–97.

[21] C. Lopes and A. Sayed, Diffusion least-mean squares over adaptive networks: formulation and performance analysis, *IEEE Trans. Signal Process*., 56 (2008), 3122–36. https://doi.org/10.1109/TSP.2008.917383

[22] J. Lorente, C. Antonanzas, M. Ferrer, and A. Gonzalez, Block-based distributed adaptive filter for active noise control in a collaborative network, *23rd Euro. Signal Process. Conf. (EUSIPCO)*, Nice, France, 31 Aug. – 4. Sep., 2015.

[23] M. Ferrer, A. Gonzalez, M. de Diego, and G. Piñero, Distributed affine projection algorithm over acoustically coupled sensor networks, *IEEE Trans. Signal Process*., 65 (2017), 6423–6434. https://doi.org/10.1109/TSP.2017.2742987

[24] S. C. Chan and Y. J. Chu, Performance analysis and design of FxLMS algorithm in broadband ANC system with online secondary-path modeling, *IEEE Trans. Audio, Speech, Lang. Process.*, vol. 20 (3) (2012) 982–993. https://doi.org/ 10.1109/TASL.2011.2169789

[25] Y. Gao, J. Ni, J. Chen, and X. Chen, Steady-state and stability analyses of diffusion sign-error LMS algorithm, *Signal Process.*, 149 (2018), 62–67. https://doi.org/10.1016/j.sigpro.2018.02.033

[26] J. Chen, C. Richard, and A. Sayed, Diffusion LMS over multitask networks, *IEEE Trans. Signal Process.*, 63 (2015), 2733–2748. https://doi.org/10.1109/TSP.2015.2412918

[27] B. Widrow, J. M. McCool, M. G. Larimore, and C. R. Johnson, Jr., Stationary and nonstationary learning characteristics of the LMS adaptive filter, in *Proc. IEEE*, 64 (1976), 1151–1162. https://doi.org/10.1109/PROC.1976.10286

[28] S. Haykin, *Adaptive Filter Theory*. 4th edition, Prentice Hall, 2001.

[29] F. S. Cattivelli, C. G. Lopes, and A. H. Sayed, Diffusion recursive least-squares for distributed estimation over adaptive networks, *IEEE Trans. Signal Process.*, 56 (2008), 1865–1877. https://doi.org/10.1109/TSP.2007.913164
[30] Y. J. Chu, A new regularized subband ANC algorithm with online secondary-path modeling: Performance analysis and application to buildings. *Build. Environ*., 94 (2015) 873–82. https://doi.org/10.1016/j.buildenv.2015.07.009
[31] R. Delegà, G. Bernasconi, L. Piroddi, A novel cost-effective parallel narrowband ANC system with local secondary-path estimation, *J. Sound Vib*. 401 (2017) 311–325. https://doi.org/10.1016/j.jsv.2017.04.034
[32] R. H. Kwong and E. W. Johnston, A variable step size LMS algorithm, *IEEE Trans. Signal Process.*, 40 (1992), 1633–1642. https://doi.org/10.1109/78.143435